Theoretical Aerodynamics of One-Lobed Flexible Parawings at Low Speeds

JACK N. NIELSEN,* ANTHONY R. KRIEBEL,† and FREDERICK K. GOODWIN‡
Itek Corporation, Palo Alto, Calif.

This paper presents a theoretical treatment of the problem of determining the shape and aerodynamic characteristics of a one-lobed flexible parawing. A general theory is developed utilizing slender-body theory and is then linearized. From this theory it is possible to obtain shapes and aerodynamic characteristics in nondimensional form as a function of only one variable. The results of calculations that have been made are presented in tabular form. An example of how these results can be applied to a specific parawing is presented.

Nomenclature

a_n = complex coefficients in Eq. (5)
$b_{2j.m}$ = coefficients defined by Eq. (26)
c = local chord of parawing
c_r = root chord of parawing
c_l = section lift coefficient of streamwise section
c_{2j} = Fourier coefficients in series defining shape of parawing
C_{D_i} = $D_i/(\frac{1}{2})\rho V^2 S$
C_{D_P} = $D_P/(\frac{1}{2})\rho V^2 S$
C_{D_S} = $D_S/(\frac{1}{2})\rho V^2 S$
C_L = lift coefficient of parawing
$d_{2j.m}$ = coefficients defined by Eq. (26)
D_i = induced drag of parawing
D_P = pressure drag of parawing, no leading-edge suction
D_S = pressure drag of parawing due to leading-edge suction
K_{ij} = coefficients of c_{2j} matrix
l = length of membrane between $y = -s$ and $y = +s$ in crossflow plane
Δp = difference in static pressure between upper and lower surfaces
p = local static pressure
p_n, q_n = $a_n = p_n + iq_n$
P = pressure coefficient $(p - p_\infty)/(\frac{1}{2})\rho V^2$
P_{2n} = $(2n/s)(2/s)^{2n}p_{2n}$
ΔP = $P^- - P^+$
P^+, P^- = pressure coefficients on lower and upper surfaces, respectively
q = dynamic pressure, $(\frac{1}{2})\rho V^2$
Q_{2n} = $(2n/s)(2/s)^{2n}q_{2n}$
r = radius in σ plane
r_0 = radius of circle into which wing section is mapped in σ plane
s = local semispan of parawing
S = wing planform area
T = spanwise tension in wing membrane per unit streamwise distance
T^* = $T/4\ sq\ \tan\epsilon$
u, v, w = velocity perturbations along x, y, and z, respectively
u^+, v^+, w^+ = value of u, v, w on lower surface
u^-, v^-, w^- = values of u, v, w on upper surface
u_s, v_s, w_s = part of u, v, w even top to bottom of wing
u_u, v_u, w_u = part of u, v, w odd top to bottom of wing
V = freestream velocity
W = complex potential, $\phi + i\psi$, for u, v, w
α = angle of attack
ϵ = semiapex angle of parawing planform
ζ = $y + iz$
η = distance of parawing surface above chord plane
θ = polar angle in σ plane
λ = tension parameter, $T/4\ sq\ \tan^2\epsilon$
ρ = mass density of air
ϕ = potential function for u, v, w
ϕ_{le}, ϕ_{te} = values of ϕ at leading edge or trailing edge
ψ = stream function in $W = \phi + i\psi$

Received November 7, 1963; revision received October 5, 1964. This work was performed under Contract No. Nonr 3728(00) sponsored by Air Programs, Office of Naval Research, Washington, D. C.

* Director, Research and Development Branch, Vidya Division. Associate Fellow Member AIAA.
† Staff Scientist, Vidya Division. Member AIAA.
‡ Head, Numerical Analysis Section, Vidya Division. Member AIAA.

1. Introduction

THE theoretical aerodynamics of streamline shapes has been developed almost entirely for rigid rather than flexible bodies. For rigid bodies the problem is usually to determine the pressure distribution given a shape, or conversely. Aeroelastic analysis that considered small deformations from a rigid shape is a partial exception to the general rule, as well as the specialized studies of parachute shapes during inflation. It can, however, be said that very little attention has been paid to the aerodynamics of flexible bodies in steady flight where the aerodynamic shape and loading are directly related to each other in a first-order fashion. Examples of such flexible bodies include ship sails, the Rogallo wing (parawing), and flexible rotors.

Recently, several papers have appeared in the literature that treats the theoretical aerodynamics of two-dimensional sails.[1, 2] The interesting thing about these analyses is that the solutions exhibit certain eigenvalue shapes for certain eigenvalues of a nondimensional parameter involving the tension in the flexible surface. The method used in Ref. 2 appears applicable to three-dimensional slender wings through the use of slender-body theory. It is the purpose of this paper to attempt slender-body solutions for the case of slender delta parawings. Also, it appears that the two-dimensional sail theory can be used as a basis of three-dimensional flexible wing theory through the use of strip theory. This paper is an abbreviated version of Ref. 3.

2. Analysis of Parawing

2.1 General Approach

Consider a slender, conical, one-lobed parawing, of the type shown in Fig. 1. The problem is to find the shape of the membrane surface and the corresponding aerodynamic loading as functions of α and ϵ. The procedure to be followed will be to relate the surface geometric characteristics, through the appropriate boundary conditions and tension conditions to sidewash and downwash perturbation velocities from which the potential function can be formed. From the potential function, the longitudinal perturbation velocity which is necessary to determine the surface pressures can be derived.

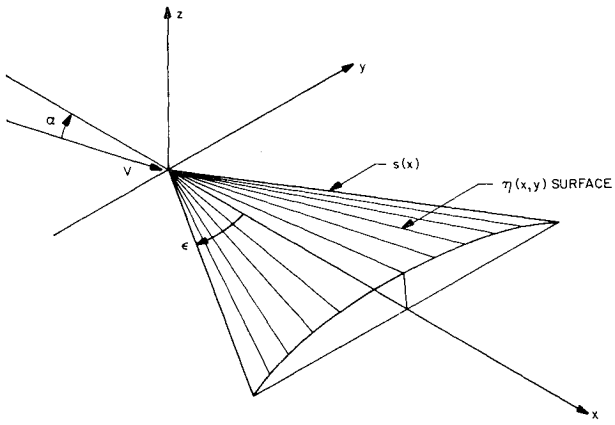

Fig. 1 Axes and notation for conical parawing.

From the surface pressures, the aerodynamic lift and drag coefficients can be determined. We will use the body centered coordinates (x, y, z) as shown. The corresponding components of the velocity perturbations are (u, v, w) as given by the perturbation velocity potential ϕ. In Ref. 3 it is shown that the boundary condition is

$$(w/V) + \alpha = (v/V)\eta_y + \eta_x \tag{1}$$

Also, in Ref. 3, it is shown that there is no tension in the membrane in the x direction, that the tension T in the y direction is a function only of x, and that the equation for equilibrium between the membrane loading and its spanwise tension is

$$\Delta p = -T\eta_{yy} \tag{2}$$

where Δp is the difference between the pressure on the lower surface and on the upper surface.

The shape of the surface is assumed to be conical, as given by

$$\eta = s \sum_{j=1}^{\infty} c_{2j}(1 - \cos 2j\theta) \tag{3}$$

where

$$s = x \tan\epsilon \qquad y = s\cos\theta \tag{4}$$

and c_0 has been chosen so that $\eta(0) = \eta(\pi) = 0$.

Let us now transform the wing surface in any y, z plane into a circle in the σ plane by means of the transformation shown in Fig. 2. Then the complex perturbation potential for the crossflow velocity field in the transformed (σ) coordinate system for unit V is given by the equation

$$W = \phi + i\psi = \sum_{n=1}^{\infty} \frac{a_n}{\sigma^n} \tag{5}$$

Equations (1, 3, and 5) and (2, 3, and 5) will each yield a set of simultaneous equations from which the coefficients c_{2j} and a_n can be found.

2.2 Slopes and Curvatures

The slopes η_x and η_y and the y curvature required in Eqs. (1) and (2) can be obtained from Eqs. (3) and (4). These are found to be

$$\eta_x = \frac{\partial\eta}{\partial x} = \tan\epsilon\left[\sum_{j=1}^{\infty} c_{2j}(1 - \cos 2j\theta + 2j \operatorname{ctn}\theta \sin 2j\theta)\right] \tag{6}$$

$$\eta_y = \frac{\partial\eta}{\partial y} = -\frac{1}{\sin\theta}\sum_{j=1}^{\infty} 2jc_{2j}\sin 2j\theta \tag{7}$$

$$\eta_{yy} = \frac{\partial^2\eta}{\partial y^2} = -\frac{1}{s\sin^2\theta}\sum_{j=1}^{\infty} 2jc_{2j}(\operatorname{ctn}\theta \sin 2j\theta - 2j\cos 2j\theta) \tag{8}$$

2.3 Perturbation Velocity Components

Let us now develop relationships for the perturbation velocities. From Eq. (5),

$$\frac{dW}{d\zeta} = \frac{v}{V} - i\frac{w}{V}$$

and from the transformation on $|\sigma|$ equal unity

$$\frac{dW}{d\sigma} = \frac{dW}{d\zeta}\frac{d\zeta}{d\sigma} = \left(\frac{v}{V} - i\frac{w}{V}\right)\left(2ie^{-i\theta}\sin\theta\right) \tag{9}$$

Also from Eq. (5) in terms of the series for W

$$\frac{dW}{d\sigma} = -\sum_{n=1}^{\infty} na_n\left(\frac{s}{2}\right)^{-(n+1)} e^{-i(n+1)\theta} \tag{10}$$

Let the complex coefficients a_n be defined as

$$a_n \equiv p_n + iq_n \tag{11}$$

Then by equating Eqs. (9) and (10) and using Eq. (11) we find

$$\left.\begin{aligned} \frac{w}{V} &= -\frac{1}{s\sin\theta}\sum_{n=1}^{\infty} n\left(\frac{2}{s}\right)^n (p_n \cos n\theta + q_n \sin n\theta) \\ \frac{v}{V} &= \frac{1}{s\sin\theta}\sum_{n=1}^{\infty} n\left(\frac{2}{s}\right)^n (p_n \sin n\theta - q_n \cos n\theta) \end{aligned}\right\} \tag{12}$$

2.4 Velocities and Potential for Vertical Plane of Symmetry

Because of the required symmetry of the flow about the midspan in both the horizontal and vertical directions, certain of the terms in Eq. (12) can be eliminated. From these symmetry arguments Eq. (12) reduces to

$$\left.\begin{aligned} \frac{w}{V} &= -\frac{1}{\sin\theta}\sum_{n=1}^{\infty} [p_{2n}\cos 2n\theta + Q_{2n-1}\sin(2n-1)\theta] \\ \frac{v}{V} &= \frac{1}{\sin\theta}\sum_{n=1}^{\infty} [P_{2n}\sin 2n\theta - Q_{2n-1}\cos(2n-1)\theta] \end{aligned}\right\} \tag{13}$$

where

$$P_{2n} \equiv \frac{2n}{s}\left(\frac{2}{s}\right)^{2n} p_{2n} \qquad Q_{2n-1} \equiv \left(\frac{2n-1}{s}\right)\left(\frac{2}{s}\right)^{2n-1} q_{2n-1} \tag{14}$$

Since the expressions for v and w [Eq. (13)] do not contain all of the p_n and q_n coefficients of Eq. (11), the complex perturbation potential with a vertical plane of symmetry is

$$\begin{aligned} \frac{W}{V} &= \sum_{n=1}^{\infty}\left(\frac{p_{2n}}{\sigma^{2n}} + i\frac{q_{2n-1}}{\sigma^{2n-1}}\right) \\ &= \sum_{n=1}^{\infty}\left\{p_{2n}\left(\frac{2}{s}\right)^{2n}(\cos 2n\theta - i\sin 2n\theta) + iq_{2n-1}\left(\frac{2}{s}\right)^{2n-1}[\cos(2n-1)\theta - i\sin(2n-1)\theta]\right\} \end{aligned}$$

and the corresponding potential function is

$$\phi = \sum_{n=1}^{\infty}\left[\frac{s}{2n}P_{2n}\cos 2n\theta + \frac{s}{2n-1}Q_{2n-1}\sin(2n-1)\theta\right] \tag{15}$$

In order to determine the expression for the loading, the expression for the u component of velocity is needed:

$$u = \frac{\partial\phi(s,\theta)}{\partial x} = \frac{\partial\phi}{\partial s}\frac{\partial s}{\partial x}\bigg|_y + \frac{\partial\phi}{\partial\theta}\frac{\partial\theta}{\partial x}\bigg|_y \tag{16}$$

From Eqs. (4) and (15),

$$u = \tan\epsilon \sum_{n=1}^{\infty} \left[\frac{P_{2n}}{2n} \cos 2n\theta + \frac{Q_{2n-1}}{2n-1} \sin(2n-1)\theta \right] + \frac{\tan\epsilon \cos\theta}{\sin\theta} \sum_{n=1}^{\infty} \left[-P_{2n} \sin 2n\theta + Q_{2n-1} \cos(2n-1)\theta \right] \quad (17)$$

2.5 Loading Equation

In this derivation of the loading equation confine attention to the internal $0 \leq \theta \leq \pi$ which, from the transformation, contains the upper surface. Let u^-, v^-, w^- be the values of u, v, w on this surface and u^+, v^+, w^+ be the values on the lower surface. Let the subscripts u and s designate components that are unsymmetrical and symmetrical with respect to the upper and lower surfaces. Then

$$u^- = u_s{}^- + u_u{}^- \qquad v^- = v_s{}^- + v_u{}^- \qquad w^- = w_s{}^- + w_u{}^- \quad (18)$$

From Eq. (3-52) of Ref. 4, the pressure coefficient can be written as

$$P = -2(u + \alpha w) - (v^2 + w^2)$$

and since

$$u_s{}^+ = u_s{}^- \qquad u_u{}^+ = -u_u{}^-$$
$$v_s{}^+ = v_s{}^- \qquad v_u{}^+ = -v_u{}^-$$
$$w_s{}^+ = w_s{}^- \qquad w_u{}^+ = -w_u{}^-$$

we obtain for the loading coefficient

$$\Delta P = P^+ - P^- = 4(u_u{}^- + \alpha w_u{}^- + v_u{}^- v_s{}^- + w_u{}^- w_s{}^-) \quad (19)$$

From Eqs. (13) and (17)

$$\left.\begin{aligned} u_u{}^- &= \tan\epsilon \sum_{n=1}^{\infty} \left[\frac{Q_{2n-1}}{2n-1} \sin(2n-1)\theta + \frac{\cos\theta}{\sin\theta} Q_{2n-1} \cos(2n-1)\theta \right] \\ v_u{}^- &= -\sum_{n=1}^{\infty} Q_{2n-1} \frac{\cos(2n-1)\theta}{\sin\theta} \\ v_s{}^- &= -\sum_{n=1}^{\infty} P_{2n} \frac{\sin 2n\theta}{\sin\theta} \\ w_u{}^- &= -\sum_{n=1}^{\infty} P_{2n} \frac{\cos 2n\theta}{\sin\theta} \\ w_s{}^- &= -\sum_{n=1}^{\infty} Q_{2n-1} \frac{\sin(2n-1)\theta}{\sin\theta} \end{aligned}\right\} \quad (20)$$

so that

$$\sin^2\theta \frac{\Delta p}{q} = -\left[-4 \tan\epsilon \sin^2\theta \sum_{n=1}^{\infty} \frac{Q_{2n-1}}{2n-1} \sin(2n-1)\theta - 4 \tan\epsilon \sin\theta \cos\theta \sum_{n=1}^{\infty} Q_{2n-1} \cos(2n-1)\theta + 4\alpha \sin\theta \sum_{n=1}^{\infty} P_{2n} \cos 2n\theta + 4 \sum_{n=1}^{\infty} P_{2n} \sin 2n\theta \sum_{m=1}^{\infty} Q_{2m-1} \cos(2m-1)\theta - 4 \sum_{n=1}^{\infty} P_{2n} \cos 2n\theta \sum_{m=1}^{\infty} Q_{2m-1} \sin(2m-1)\theta \right] \quad (21)$$

The multiplication by $\sin^2\theta$ is performed in order to remove the leading-edge singularity.

From Eqs. (2) and (8), we can find another equation for the loading in terms of the shape:

$$\sin^2\theta \frac{\Delta p}{q} = -\frac{T}{sq} \left[\sum_{j=1}^{\infty} (2j)^2 c_{2j} \cos 2j\theta - \sum_{j=1}^{\infty} 2jc_{2j} \frac{\cos\theta \sin 2j\theta}{\sin\theta} \right] \quad (22)$$

2.6 Linearized Solution

It is to be noted that the loading as given by Eq. (21) contains nonlinear terms corresponding to doubly infinite series involving products of P_{2n} and Q_{2n-1}. Also, the boundary condition, Eq. (1), contains a nonlinear term in $(v/V)\eta_y$. If we drop the nonlinear terms, Eqs. (1) and (19) become

$$\frac{w}{V} + \alpha = \eta_x \qquad \Delta P = \frac{\Delta p}{q} = 4u_u{}^- \quad (23)$$

Upon substituting the unsymmetrical $u_u{}^-$ part of Eq. (20) into Eq. (23), we have

$$\sin^2\theta \frac{\Delta p}{q} = 4 \sin^2\theta \tan\epsilon \sum_{n=1}^{\infty} \frac{Q_{2n-1}}{2n-1} \sin(2n-1)\theta + 4 \sin\theta \cos\theta \tan\epsilon \sum_{n=1}^{\infty} Q_{2n-1} \cos(2n-1)\theta \quad (24)$$

If Eqs. (22) and (24) are expanded as sine series over the interval $0 \leq \theta \leq \pi$ and the resulting equations equated, we obtain

$$\frac{T}{4sq \tan\epsilon} \sum_{j=1}^{\infty} 2jc_{2j} \sum_{k=1}^{\infty} a_{2j,\,2k-1} \sin(2k-1)\theta = -\sum_{n=1}^{\infty} \frac{Q_{2n-1}}{2n-1} \left[\frac{1}{2} \sin(2n-1)\theta + \frac{(n-1)}{2} \sin(2n+1)\theta - \frac{n}{2} \sin(2n-3)\theta \right] \quad (25)$$

where

$$\left.\begin{aligned} a_{2j,\,2k-1} &= 2jb_{2j,\,2k-1} - d_{2j,\,2k-1} \\ 2jb_{2j,\,2k-1} &= \frac{4}{\pi} \left[\frac{2j(2k-1)}{(2k-1)^2 - (2j)^2} \right] \\ d_{2j,\,2k-1} &= \frac{2}{\pi} \left[\sum_{i=1,3,5}^{|2j+2k|-1} \frac{1}{i} - \sum_{i=1,3,5}^{|2j-2k+2|-1} \frac{1}{i} + \sum_{i=1,3,5}^{|2j+2k-2|-1} \frac{1}{i} - \sum_{i=1,3,5}^{|2j-2k|-1} \frac{1}{i} \right] \end{aligned}\right\} \quad (26)$$

Let

$$T^* = T/4\,sq \tan\epsilon$$

If Eq. (25) is expanded and the coefficients of like sine terms

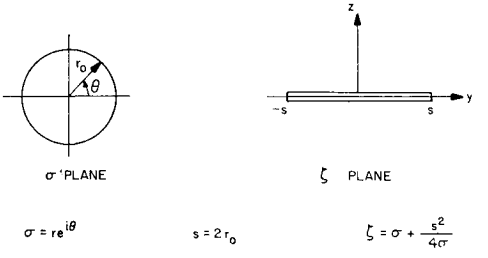

Fig. 2 Transformation.

equated, the following set of simultaneous equations is obtained:

$$
\begin{aligned}
&\text{Sin}\theta \\
&T^*(2c_2a_{21} + 4c_4a_{41} + 6c_6a_{61} + \dots) = -\left(Q_1 - \frac{Q_3}{3}\right) \\
&\text{Sin}3\theta \\
&T^*(2c_2a_{23} + 4c_4a_{43} + 6c_6a_{63} + \dots) = \\
&\qquad -\left(\frac{Q_3}{6} - \frac{3}{10}Q_5\right) \\
&\text{Sin}5\theta \\
&T^*(2c_2a_{25} + 4c_4a_{45} + 6c_6a_{65} + \dots) = \\
&\qquad -\left(\frac{Q_3}{6} + \frac{Q_5}{10} - \frac{2Q_7}{7}\right) \\
&\text{Sin}7\theta \\
&T^*(2c_2a_{27} + 4c_4a_{47} + 6c_6a_{67} + \dots) = \\
&\qquad -\left(\frac{Q_5}{5} + \frac{Q_7}{14} - \frac{5Q_9}{18}\right) \\
&\text{Sin}m\theta \\
&T^*(2c_2a_{2m} + 4c_4a_{4m} + 6c_6a_{6m} + \dots) = - \\
&\qquad \left[\frac{Q_{m-2}}{4}\left(1 - \frac{1}{m-2}\right) + \frac{Q_m}{2}\left(\frac{1}{m}\right)\right. \\
&\qquad \left. - \frac{Q_{m+2}}{4}\left(\frac{1}{m+2} + 1\right)\right]
\end{aligned}
\qquad (27)
$$

A set of simultaneous equations has thus been obtained from the loading equation. In a similar manner another set can be obtained from the boundary condition [Eq. (23)] and Eqs. (6) and (13). This set is

$$
\begin{aligned}
&-Q_1 + \sin\alpha = \tan\epsilon\left(\tfrac{5}{2}c_2 + c_4 + c_6 + \dots\right) \\
&-Q_3 = \tan\epsilon\left(\frac{c_2}{2} + \frac{5}{2}c_4\right) \\
&-Q_5 = \tan\epsilon\left(\frac{3}{2}c_4 + \frac{7}{2}c_6\right) \\
&-Q_7 = \tan\epsilon\left(\frac{5}{2}c_6 + \frac{9}{2}c_8\right) \\
&\qquad \vdots \\
&-Q_n = \tan\epsilon\left(\frac{n-2}{2}c_{n-1} + \frac{n+2}{2}c_{n+1}\right)
\end{aligned}
\qquad (28)
$$

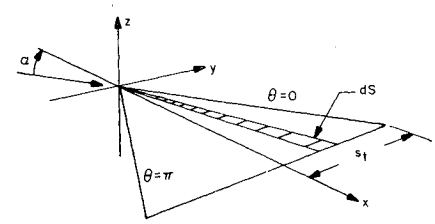

Fig. 3 Notation for pressure-drag calculation.

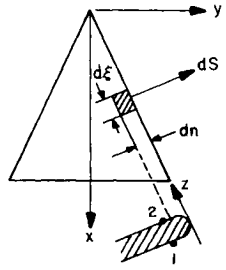

Fig. 4 Notation for leading-edge suction calculation.

Let

$$\lambda \equiv \frac{T}{4 \text{ sq } \tan^2\epsilon}$$

By substituting Eq. (28) into Eq. (27) the following set of equations which determine the c_j's is obtained:

$j \backslash n$	1	2	3	4	N
1	$K_{11}c_2$	$+ K_{21}c_4$	$+ K_{31}c_6$	$+ K_{41}c_8 + \dots +$	$K_{N,1}c_{2N} = -(\sin\alpha/\tan\epsilon)$
2	$K_{12}c_2$	$+ K_{22}c_4$	$+ K_{32}c_6$	$+ K_{42}c_8 + \dots +$	$K_{N,2}c_{2N} = 0$
3	$K_{13}c_2$	$+ K_{23}c_4$	$+ K_{33}c_6$	$+ K_{43}c_8 + \dots +$	$K_{N,3}c_{2N} = 0$
4	$K_{14}c_2$	$+ K_{24}c_4$	$+ K_{34}c_6$	$+ K_{44}c_8 + \dots +$	$K_{N,4}c_{2N} = 0$
.	.	.	.	.	.
.	.	.	.	.	.
.	.	.	.	.	.
J	$K_{1J}c_2$	$+ K_{2J}c_4$	$+ K_{3J}c_6$	$+ K_{4J}c_8 + \dots +$	$K_{NJ}c_{2N} = 0$

(29)

The K_{nj}'s are given by the following expressions:

$j = 1$

$n = 1 \qquad K_{11} = 2a_{21}\lambda - \frac{7}{3}$

$n = 2 \qquad K_{21} = 4a_{41}\lambda - \frac{1}{6}$

$n = 3 \rightarrow N \qquad K_{n,1} = 2na_{2n,1}\lambda - 1$

$j = 2$

$n = 1 \qquad K_{12} = 2a_{23}\lambda - \frac{1}{12}$

$n = 2 \qquad K_{22} = 4a_{43}\lambda + \frac{1}{30}$

$n = 3 \qquad K_{32} = 6a_{63}\lambda + \frac{21}{20}$

$n = 4 \rightarrow N \qquad K_{n,2} = 2na_{2n,3}\lambda$

$j = 3 \rightarrow J$

$n \neq (j-2), (j-1), j, (j+1) \qquad K_{nj} = 2na_{2n,2j-1}\lambda$

$$n = j - 2 \qquad K_{j-2,j} = 2(j-2)a_{2(j-2),\,2j-1}\lambda - \frac{(2j-5)}{8}\left(1 - \frac{1}{2j-3}\right)$$

$$n = j - 1 \qquad K_{j-1,\,j} = 2(j-1)a_{2(j-1),\,2j-1}\lambda - \frac{(2j-1)}{8}\left(1 - \frac{1}{2j-3}\right) - \frac{(2j-3)}{4}\left(\frac{1}{2j-1}\right)$$

$$n = j \qquad K_{jj} = 2ja_{2j,\,2j-1}\lambda - \frac{(2j+1)}{4(2j-1)} + \frac{(2j-1)}{8}\left(\frac{1}{2j+1} + 1\right)$$

$$n = j + 1 \qquad K_{j+1,\,j} = 2(j+1)a_{2(j+1),\,2j-1}\lambda + \frac{(2j+3)}{8}\left(\frac{1}{2j+1} + 1\right)$$

The a_{nj}'s are given by Eq. (26).

The linearized solution is found by solving Eq. (29) for the c's, and then Eq. (28) for the Q's.

2.7 Lift and Drag for Linearized Solution

2.7.1 *Lift coefficient*

The lift coefficient of the wing is obtained by direct integration of the pressure over the surface. The lift coefficient of a local strip is given by

$$c_l = \frac{1}{c}\int_{le}^{te} \Delta P\, dx = \frac{4}{c}\int_{le}^{te} \frac{\phi_x^-}{V}\, dx \tag{30}$$

From Eq. (15) we find that

$$\frac{\phi^-}{V} = \sum_{n=1}^{\infty} \frac{s}{2n-1} Q_{2n-1} \sin(2n-1)\theta \tag{31}$$

so that Eq. (30) yields, for the section lift coefficient,

$$c_l = \frac{4\tan\epsilon}{1-\cos\theta} \sum_{n=1}^{\infty} \frac{Q_{2n-1}}{2n-1} \sin(2n-1)\theta \tag{32}$$

To obtain the total lift force it is now necessary to integrate $c_l c$ across the trailing edge. Thus,

$$C_L = \frac{1}{S_W}\int_{-s_t}^{s_t} cc_l\, dy = 2\pi \tan\epsilon\, Q_1 \tag{33}$$

2.7.2 *Induced drag*

The induced drag represents the sole drag in the present potential flow analysis. It can be evaluated from the results of Ref. 5. For circulation distribution with a semispan s given by

$$\Gamma = 4sV \sum_{n=1}^{\infty} A_n \sin n\theta \tag{34}$$

the induced drag is given by

$$D_i = 2\pi\rho s^2 V^2 \sum_{n=1}^{\infty} nA_n{}^2 \tag{35}$$

Since we know that the circulation distribution is given by

$$\Gamma = 2\phi_{te}{}^- = 2sV \sum_{n=1}^{\infty} \frac{Q_{2n-1}}{2n-1} \sin(2n-1)\theta$$

by analogy the induced drag is

$$C_{D_i} = \frac{D_i}{(s^2/\tan\epsilon)(\rho V^2/2)} = \pi \tan\epsilon \sum_{n=1}^{\infty} \frac{Q_{2n-1}{}^2}{2n-1} \tag{36}$$

2.7.3 *Pressure drag, no leading-edge suction*

The pressure drag component without the leading-edge suction is found by direct integration of the pressure distribution over the surface of the wing. The drag per unit area is the loading on that area times its inclination in the drag direction. With reference to Fig. 3 the drag integral can be written

$$D_P = \int_0^{S_W} \Delta P \left(\alpha - \frac{d\eta}{dx}\, dS\right) \tag{37}$$

and in coefficient form becomes

$$C_{D_P} = \frac{D_P}{qS_W} = \frac{1}{2}\int_0^{\pi} \Delta P \left(\alpha - \frac{d\eta}{dx}\right) \sin\theta\, d\theta \tag{38}$$

Using Eqs. (6) and (20) and carrying out the integration yields

$$\frac{C_{D_P}}{\sin^2\alpha\tan\epsilon} = \frac{C_L}{\sin\alpha\tan\epsilon}\left(1 - \sum_{j=1}^{\infty} c_{2j}{}'\right) + \frac{\pi}{2}\sum_{j=1}^{\infty} c_{2j}{}'\left(-\frac{Q_{2j-1}{}'}{2j-1} + Q_{2j-1}{}' + \frac{Q_{2j+1}{}'}{2j+1} + Q_{2j+1}{}'\right) - \frac{\pi}{2}\sum_{j=1}^{\infty} 2jc_{2i}{}'\left(\frac{Q_{2j-1}{}'}{2j-1} - Q_{2j-1}{}' + \frac{Q_{2j+1}{}'}{2j+1} + Q_{2j+1}{}'\right) - 2\pi\sum_{j=1}^{\infty} 2jc_{2j}{}' \sum_{n=1}^{j} Q_{2n-1}{}' \tag{39}$$

2.7.4 *Leading-edge suction*

Because of the leading-edge suction, a finite thrust actually occurs at the leading edge tending to reduce the pressure drag calculated in the preceding section. In fact, the induced drags and pressure drags are equal when account is taken of leading-edge suction

$$C_{D_i} = C_{D_P} + C_{D_S} \tag{40}$$

The suction force for a small area of leading edge is (Fig. 4)

$$dD_S/d\xi = \int p[\alpha - (d\eta/dx)] \cos\epsilon\, dy \tag{41}$$

The linearized boundary condition and pressure relationship

$$\alpha - (d\eta/dx) = -w/V \qquad p = -2\rho_\infty(u/V) \tag{42}$$

yield

$$\frac{dD_S}{d\xi} = 2\rho_\infty \int_1^2 \frac{u}{V}\frac{w}{V}\cos\epsilon\, dy \tag{43}$$

where the limits are the ends of the contour around the leading edge.

In the neighborhood of the leading edge ($\theta = 0$), we find that the dominant terms in u and v from Eq. (20) yield

$$u = -v\tan\epsilon \tag{44}$$

so that the drag integral becomes

$$\frac{dD_S}{d\xi} = -2\sin\epsilon\rho_\infty \int_1^2 \frac{v}{V}\frac{w}{V}\, dy \tag{45}$$

We now make use of a result of Jones and Cohen[6] that proves that, if $v - iw$ is an analytic function of $x + iy$, then integral I around a leading-edge square-root singularity at $x = 0$ is given by

$$I = \int uw\, dx = (\pi/2)C^2 \tag{46}$$

where

$$C = \lim_{x\to 0} u(x)^{1/2} \tag{47}$$

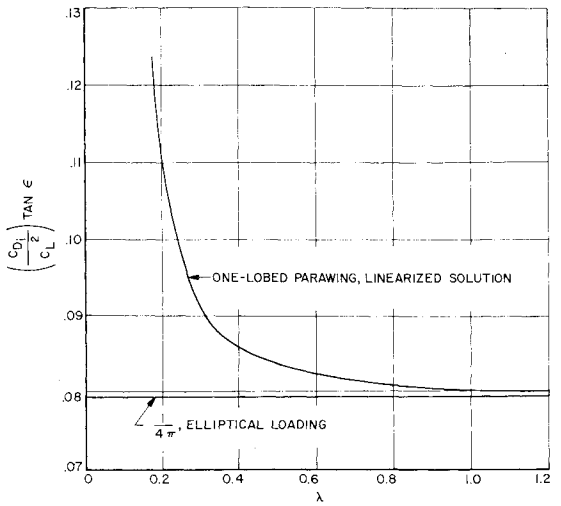

Fig. 5 Induced-drag factor for one-lobed delta parawings.

In the present case $v - iw$ is an analytic function of $y + iz$ with a square-root singularity at $y = s$:

$$v(s - y)^{1/2} \rightarrow \frac{s}{(2s)^{1/2}} \sum_{n=1}^{\infty} Q_{2n-1} \text{ as } s \rightarrow y \tag{48}$$

so that

$$C^2 = \frac{s}{2}\left(\sum_{n=1}^{\infty} Q_{2n-1}\right)^2$$

Thus, the drag per unit length of the leading edge becomes

$$\frac{dD_S}{d\xi} = -\pi\left(\frac{\rho_\infty}{2} V^2\right) s \sin\epsilon \left(\sum_{n=1}^{\infty} Q_{2n-1}\right)^2$$

and

$$C_{D_S} = \frac{D_S}{[(\rho_\infty/2)V^2][(s_t^2/\tan\epsilon)]} = -\pi \tan\epsilon \left(\sum_{n=1}^{\infty} Q_{2n-1}\right)^2 \tag{49}$$

2.8 Slack Parameter

The two parameters that can be considered to determine the aerodynamic coefficients of a one-lobed parawing are the angle of attack and the slack parameter. The slack parameter is defined to be $(l - 2s)/2s$. The length of the membrane l between $y = -s$ and $y = +s$ in any yz plane is

$$l = \int_{-s}^{s} \left[1 + \left(\frac{d\eta}{dy}\right)^2\right]^{1/2} dy$$

Assuming $d\eta/dy$ to be small, we find that

$$\left(\frac{l - 2s}{2s}\right) = \frac{1}{4}\int_{-1}^{+1} \left(\frac{d\eta}{dy}\right)^2 d\left(\frac{y}{s}\right) \tag{50}$$

Substituting $d\eta/dy$ from Eq. (7) into Eq. (50) and carrying out the integration we have

$$\left(\frac{l - 2s}{2s}\right)\left(\frac{\tan\epsilon}{\sin\alpha}\right)^2 = \frac{1}{2}\sum_{j=1}^{\infty} (2j)^2 \times (c_{2j}')^2 \sum_{m=1,3,5}^{4j-1} \frac{1}{4j - m} + \sum_{j=1}^{\infty}\sum_{k=j+1}^{\infty} (2j) \times (2k) c_{2j}' c_{2k}' \sum_{m=1,3,5}^{4j-1} \frac{1}{2j + 2k - m} \tag{51}$$

3. Calculated Results for One-Lobed Parawing

3.1 Accuracy of Calculated Results

A series of calculations have been performed on the Vidya IBM 1620 computer to obtain the shapes, loadings, and other aerodynamic characteristics of a one-lobed parawing. It has been found possible to determine these quantities in nondimensional form as a function of one variable only, the tension parameter λ:

$$\lambda = T/4\, sq \tan^2\epsilon$$

In order to examine the accuracy of the calculations, the number of harmonics used in the calculation was varied. For λ greater than 0.1 it was found that 20 harmonics yield adequate accuracy for engineering purposes.

As λ approaches zero, the accuracy of the calculative scheme becomes less as shown by comparisons of calculated results for 20 and 45 harmonics in Ref. 3. For $\lambda = 10^{-}$ the gross quantities are in fair accord for $n = 20$ and $n = 45$ but the loading at $y/s = 0.95$ has reached about 10% error For $\lambda = 10^{-3}$ the shape is fairly well given over the spar except near the edge. The gross properties and the loadin are quite inaccurate at 20 harmonics and may still be at 4 harmonics.

Table 1 Nondimensional characteristics of slender one-lobed delta parawings: gross characteristics

λ	$\left(\frac{l-2s}{2s}\right)\left(\frac{\tan\epsilon}{\sin\alpha}\right)^2$	$\frac{C_L}{\tan\epsilon \sin\alpha}$	$\frac{C_{D_i}}{\tan\epsilon \sin^2\alpha}$	$\frac{C_{D_P}}{\tan\epsilon \sin^2\alpha}$	$\frac{C_{D_S}}{\tan\epsilon \sin^2\alpha}$	$\sum_{n=1}^{\infty} Q_{2n-1}$	$\frac{1}{\sin\alpha}\left(\frac{d\eta}{dx}\right)_{y=s}$	$\frac{\tan\epsilon}{\sin\alpha}\left(\frac{d\eta}{dy}\right)_{y=s}$	$\tan\epsilon \frac{C_L}{C_l}$
0.10	3.6567^{-1}	4.117^{-1}	4.8254^{-2}	5.358^{-2}	-5.333^{-3}	-4.120^{-2}	1.0393	−1.0393	0.2847
0.12	3.5288^{-1}	5.3987^{-1}	5.991^{-2}	6.690^{-2}	-7.007^{-3}	-4.723^{-2}	1.1343	−1.1343	0.2056
0.14	3.395^{-1}	6.704^{-1}	7.302^{-2}	7.902^{-2}	-6.001^{-3}	-4.371^{-2}	1.2048	−1.2048	0.1625
0.16	3.260^{-1}	7.990^{-1}	8.784^{-2}	9.159^{-2}	-3.749^{-3}	-3.455^{-2}	1.2538	−1.2538	0.1376
0.18	3.129^{-1}	9.239^{-1}	1.0433^{-1}	1.0586^{-1}	-1.5289^{-3}	-2.2060^{-2}	1.2862	−1.2862	0.1222
0.20	3.001^{-1}	1.0445	1.2234^{-1}	1.2253^{-1}	1.8252^{-4}	-7.622^{-3}	1.3066	−1.3066	0.1121
0.21	2.940^{-1}	1.1030	1.3187^{-1}	1.3187^{-1}	-8.745^{-9}	5.276^{-5}	1.3132	−1.3132	0.1084
0.4	2.025^{-1}	2.020	3.502^{-1}	4.209^{-1}	-7.067^{-2}	1.4998^{-1}	1.2534	−1.2534	0.0858
0.6	1.4451^{-1}	2.693	5.958^{-1}	8.354^{-1}	-2.397^{-1}	2.762^{-1}	1.1109	−1.1109	0.0825
0.8	1.0809^{-1}	3.183	8.204^{-1}	1.2543	-4.339^{-1}	3.717^{-1}	9.834^{-1}	-9.834^{-1}	0.0810
1.0	8.383^{-2}	3.556	1.0171	1.6403	-6.233^{-1}	4.454^{-1}	8.780^{-1}	-8.780^{-1}	0.0803
1.2	6.689^{-2}	3.849	1.1873	1.9849	-7.976^{-1}	5.039^{-1}	7.914^{-1}	-7.914^{-1}	0.0800
1.4	5.460^{-2}	4.084	1.3347	2.2894	-9.548^{-1}	5.513^{-1}	7.197^{-1}	-7.197^{-1}	0.0800
1.6	4.541^{-2}	4.779	1.4628	2.5581	−1.0954	5.905^{-1}	6.595^{-1}	-6.595^{-1}	0.0799
1.8	3.836^{-2}	4.441	1.5748	2.7957	−1.2209	6.340^{-1}	6.083^{-1}	-6.083^{-1}	0.0798
2.0	3.283^{-2}	4.580	1.6734	3.0066	−1.3332	6.514^{-1}	5.644^{-1}	-5.644^{-1}	0.0798
10	2.054^{-3}	5.858	2.731	5.347	−2.616	9.125^{-1}	1.4419^{-1}	-1.4419^{-1}	0.0790
100	2.306^{-5}	6.238	3.097	6.180	−3.084	9.907^{-1}	1.5351^{-2}	-1.5351^{-2}	0.0790

Table 2 Nondimensional characteristics of slender one-lobed delta parawings: nondimensional shapes, (η/s) $(\tan\epsilon/\sin\alpha)$

	y/s									
λ	0	0.1	0.2	0.3	0.4	0.5	0.6	0.7	0.8	0.9
0.10	7.400^{-1}	7.335^{-1}	7.137^{-1}	6.796^{-1}	6.297^{-1}	5.621^{-1}	4.752^{-1}	3.689^{-1}	2.467^{-1}	1.183^{-1}
0.12	7.224^{-1}	7.162^{-1}	6.971^{-1}	6.644^{-1}	6.168^{-1}	5.527^{-1}	4.706^{-1}	3.699^{-1}	2.524^{-1}	1.246^{-1}
0.14	7.054^{-1}	6.993^{-1}	6.808^{-1}	6.492^{-1}	6.033^{-1}	5.419^{-1}	5.634^{-1}	3.670^{-1}	2.537^{-1}	1.278^{-1}
0.16	6.890^{-1}	6.830^{-1}	6.650^{-1}	6.343^{-1}	5.899^{-1}	5.306^{-1}	4.550^{-1}	3.622^{-1}	2.526^{-1}	1.291^{-1}
0.18	6.732^{-1}	6.674^{-1}	6.498^{-1}	6.199^{-1}	5.768^{-1}	5.193^{-1}	4.462^{-1}	3.565^{-1}	2.502^{-1}	1.293^{-1}
0.20	6.580^{-1}	6.524^{-1}	6.352^{-1}	6.060^{-1}	5.640^{-1}	5.081^{-1}	4.373^{-1}	3.503^{-1}	2.470^{-1}	1.287^{-1}
0.21	6.507^{-1}	6.451^{-1}	6.281^{-1}	5.992^{-1}	5.578^{-1}	5.027^{-1}	4.328^{-1}	3.471^{-1}	2.453^{-1}	1.283^{-1}
0.4	5.357^{-1}	5.311^{-1}	5.171^{-1}	4.934^{-1}	4.596^{-1}	4.151^{-1}	3.591^{-1}	2.907^{-1}	2.089^{-1}	1.127^{-1}
0.6	4.513^{-1}	4.474^{-1}	4.355^{-1}	4.156^{-1}	3.872^{-1}	3.499^{-1}	3.032^{-1}	2.461^{-1}	1.7783^{-1}	9.690^{-2}
0.8	3.898^{-1}	3.864^{-1}	3.761^{-1}	3.589^{-1}	3.344^{-1}	3.023^{-1}	2.621^{-1}	2.131^{-1}	1.5432^{-1}	8.450^{-2}
1.0	3.430^{-1}	3.400^{-1}	3.310^{-1}	3.158^{-1}	2.943^{-1}	2.661^{-1}	2.307^{-1}	1.8771^{-1}	1.3616^{-1}	7.477^{-2}
1.2	3.062^{-1}	3.035^{-1}	2.955^{-1}	2.819^{-1}	2.627^{-1}	2.375^{-1}	2.061^{-1}	1.6773^{-1}	1.2179^{-1}	6.700^{-2}
1.4	2.765^{-1}	2.741^{-1}	2.668^{-1}	2.546^{-1}	2.373^{-1}	2.146^{-1}	1.8614^{-1}	1.5157^{-1}	1.1013^{-1}	6.067^{-2}
1.6	2.521^{-1}	2.499^{-1}	2.433^{-1}	2.321^{-1}	2.163^{-1}	1.9561^{-1}	1.6973^{-1}	1.3824^{-1}	1.0050^{-1}	5.542^{-2}
1.8	2.317^{-1}	2.296^{-1}	2.235^{-1}	2.133^{-1}	1.9875^{-1}	1.7974^{-1}	1.5598^{-1}	1.2707^{-1}	9.241^{-2}	5.100^{-2}
2.0	2.143^{-1}	2.124^{-1}	2.068^{-1}	1.9727^{-1}	1.8383^{-1}	1.6626^{-1}	1.4429^{-1}	1.1756^{-1}	8.552^{-2}	4.722^{-2}
10	5.353^{-2}	5.306^{-2}	5.165^{-2}	4.928^{-2}	4.592^{-2}	4.154^{-2}	3.607^{-2}	2.942^{-2}	2.145^{-2}	1.1896^{-2}
100	5.670^{-3}	5.621^{-3}	5.471^{-3}	5.220^{-3}	4.864^{-3}	4.401^{-3}	3.822^{-2}	3.118^{-3}	2.274^{-3}	1.2625^{-3}

Table 3 Nondimensional characteristics of slender one-lobed delta parawings: nondimensional loadings, $(1/\tan\epsilon\sin\alpha)(\Delta p/q)$

	y/s									
λ	0	0.2	0.3	0.4	0.5	0.6	0.7	0.8	0.9	0.95
0.10	5.189^{-1}	5.688^{-1}	6.307^{-1}	7.066^{-1}	7.766^{-1}	7.906^{-1}	6.580^{-1}	2.729^{-1}	-3.832^{-1}	-7.660^{-2}
0.12	6.007^{-1}	6.508^{-1}	7.132^{-1}	7.910^{-1}	8.685^{-1}	9.055^{-1}	8.252^{-1}	5.213^{-1}	-1.028^{-1}	-5.646^{-2}
0.14	6.810^{-1}	7.316^{-1}	7.946^{-1}	8.741^{-1}	9.572^{-1}	1.010	9.671^{-1}	7.285^{-1}	1.683^{-1}	-2.990^{-2}
0.16	7.588^{-1}	8.100^{-1}	8.735^{-1}	9.549^{-1}	1.0428	1.1082	1.0939	9.093^{-1}	4.217^{-1}	-1.467^{-2}
0.18	8.336^{-1}	8.855^{-1}	9.496^{-1}	1.0330	1.1251	1.2007	1.2101	1.0715	6.579^{-1}	2.710^{-1}
0.20	9.054^{-1}	9.581^{-1}	1.0228	1.1081	1.2041	1.2886	1.3183	1.2200	8.785^{-1}	5.508^{-1}
0.21	9.402^{-1}	9.932^{-1}	1.0582	1.1445	1.2425	1.3310	1.3698	1.2900	9.836^{-1}	6.874^{-1}
0.4	1.4815	1.5418	1.6114	1.7149	1.8412	1.9836	2.1390	2.3000	2.5281	2.832
0.6	1.8876	1.9437	2.017	2.134	2.281	2.459	2.687	3.0000	3.605	4.394
0.8	2.166	2.236	2.312	2.439	2.602	2.804	3.083	3.501	4.376	5.525
1.0	2.385	2.459	2.537	2.672	2.845	3.066	3.383	3.880	4.957	6.381
1.2	2.557	2.633	2.713	2.854	3.037	3.273	3.619	4.176	5.412	7.054
1.4	2.695	2.774	2.855	3.001	3.191	3.439	3.809	4.415	5.778	7.595
1.6	2.810	2.890	2.972	3.122	3.318	3.576	3.865	4.611	6.079	8.040
1.8	2.905	2.987	3.070	3.223	3.425	3.690	4.095	4.774	6.330	8.413
2.0	2.987	3.070	3.153	3.310	3.516	3.788	4.207	4.914	6.544	8.730
10	3.738	3.832	3.923	4.108	4.353	4.688	5.232	6.197	8.510	1.1650^{1}
100	3.961	4.060	4.152	4.345	4.602	4.956	5.536	6.578	9.093	1.2519^{1}

Table 4 Nondimensional characteristics of slender one-lobed delta parawings: section lift coefficients, $c_l/\sin\alpha\tan\epsilon$

	y/s									
λ	0	0.2	0.3	0.4	0.5	0.6	0.7	0.8	0.9	0.95
0.10	5.184^{-1}	5.845^{-1}	5.779^{-1}	5.300^{-1}	4.242^{-1}	2.408^{-1}	-3.859^{-2}	-4.210^{-1}	-9.151^{-1}	-1.2971
0.12	6.002^{-1}	6.864^{-1}	6.939^{-1}	6.641^{-1}	5.819^{-1}	4.268^{-1}	1.7496^{-1}	-2.011^{-1}	-7.639^{-1}	-1.2564
0.14	6.805^{-1}	7.863^{-1}	8.073^{-1}	7.950^{-1}	7.356^{-1}	6.100^{-1}	3.931^{-1}	5.051^{-1}	-4.995^{-1}	-1.0010
0.16	7.584^{-1}	8.830^{-1}	9.169^{-1}	9.213^{-1}	8.837^{-1}	7.869^{-1}	6.072^{-1}	3.100^{-1}	-1.8515^{-1}	-6.3725^{-1}
0.18	8.333^{-1}	9.760^{-1}	1.0222	1.0425	1.0257	9.5675^{-1}	8.144^{-1}	5.677^{-1}	1.4979^{-1}	-2.189^{-1}
0.20	9.053^{-1}	1.0653	1.1233	1.1586	1.1616	1.1193	1.0137	8.194^{-1}	4.908^{-1}	2.255^{-1}
0.21	9.402^{-1}	1.1086	1.1723	1.2148	1.2274	1.1980	1.1102	9.424^{-1}	6.610^{-1}	4.521^{-1}
0.4	1.4834	1.7819	1.9331	2.087	2.245	2.414	2.612	2.892	3.504	4.444
0.6	1.8810	2.275	2.489	2.723	2.987	3.300	3.707	4.329	5.673	7.59
0.8	2.170	2.633	2.893	3.186	3.526	3.943	4.502	5.376	7.267	9.930
1.0	2.390	2.905	3.201	3.538	3.935	4.431	5.106	6.172	8.402	1.1719^{1}
1.2	2.563	3.119	3.443	3.814	4.256	4.815	5.581	6.798	9.440	1.3131^{1}
1.4	2.702	3.292	3.637	4.036	4.516	5.124	5.963	6.302	1.0213^{1}	1.4272^{1}
1.6	2.817	3.434	3.798	4.220	4.729	5.378	6.278	7.717	1.0849^{1}	1.5213^{1}
1.8	2.913	3.553	3.932	4.373	4.908	5.591	6.541	8.065	1.1383^{1}	1.6003^{1}
2.0	2.995	3.654	4.046	4.504	5.059	5.772	6.765	8.360	1.1837^{1}	1.6674^{1}
10	3.749	4.588	5.100	5.709	6.462	7.444	8.834	1.1091^{1}	1.6036^{1}	2.290^{1}
100	3.973	4.866	5.414	6.068	6.879	7.941	9.449	1.1904^{1}	1.7287^{1}	2.476^{1}

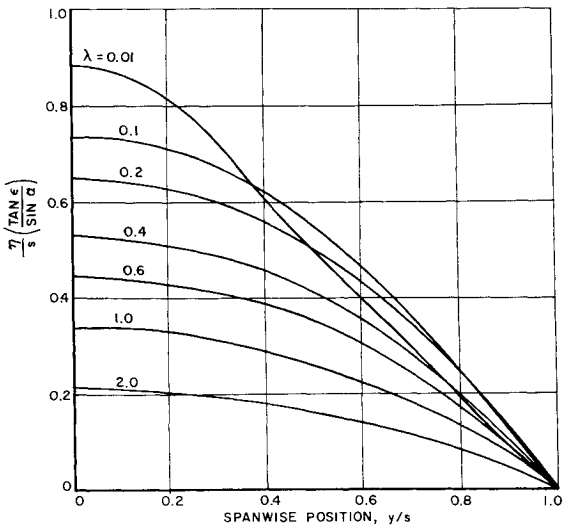

a) Upper range of λ

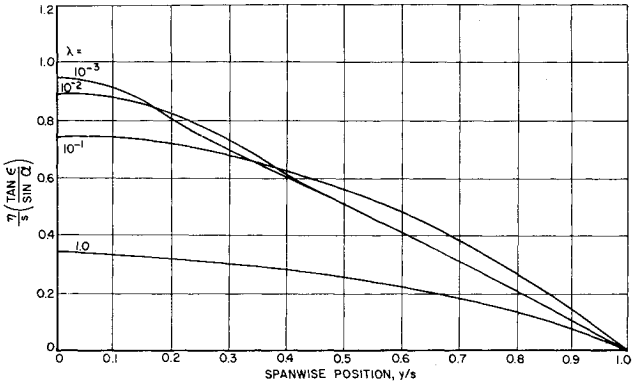

b) Low range of λ

Fig. 6 Parawing sections for one lobe.

3.2 Nondimensional Results for One-Lobed Parawings

A series of calculations has been made for various values of λ from 10^{-1} to 10^{2} which in nondimensional form completely describe the shapes and aerodynamic characteristics of all one-lobe slender parawings. These characteristics are listed in Tables 1–4 entitled gross characteristics, nondimensional shapes, nondimensional loadings, and section lift coefficients. The negative exponents indicate the power of 10 by which the tabulated values must be multiplied.

With regard to the gross characteristics, the slack for a given ϵ and α decreases as tension increases, tending to approach a flat plate, as the shapes in Table 2 show. The lift parameter increases as λ increases approaching the slender-body value of 2π. From the induced drag parameter and the lift parameter, we can form the factor $\tan\epsilon\, C_{Di}/C_L{}^2$ which for a delta wing of aspect ratio 4 $\tan\epsilon$ has a value $1/4\pi$. In Fig. 5 the value of this factor is shown vs λ.

One feature of importance is that the summation

$$\sum_{n=1}^{\infty} Q_{2n-1}$$

changes sign at $\lambda \cong 0.21$. Since the leading-edge singularity is proportional to this summation, we have a parawing with no leading-edge singularity at $\lambda \cong 0.21$. Physically, this can be interpreted to mean that the streamlines approaching the leading edge are tangent to the wing surface, and we have a condition similar to that for the ideal angle of attack for airfoils. For lesser values of λ, the loading toward the leading edge must be negative, as shown in Table 3. There is

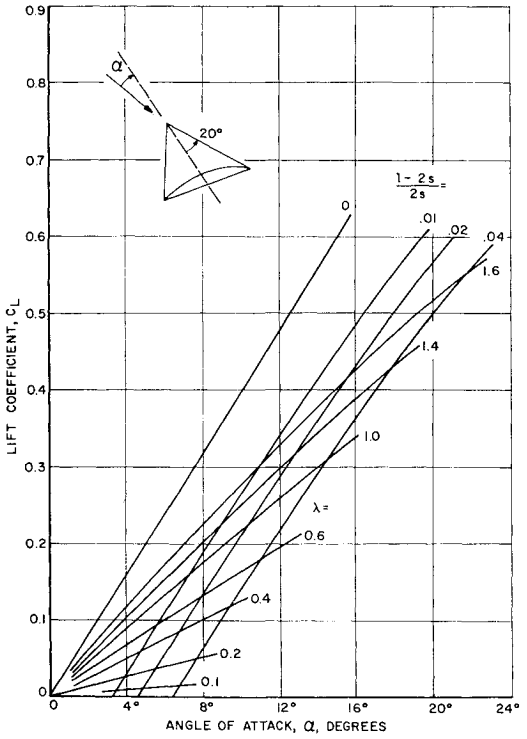

Fig. 7 Lift characteristics of one-lobed parawing with 20° semiapex angle.

thus at least one inflection point in the parawing spanwise shape for $\lambda < 0.21$. Some shapes are shown in Fig. 6.

It is of interest to examine the span loadings for the various values of λ. We put these into the form $(cc_l)/(cc_l)_0$ for ready comparison with elliptical loading values. It can be seen in Table 5 that, as the tension parameter gets larger, the span loading approaches the elliptic loading more closely.

At small values of the tension, the loading tends to be concentrated at the root chord. This effect is associated with a tendency of the surface to become flat with a ridge down

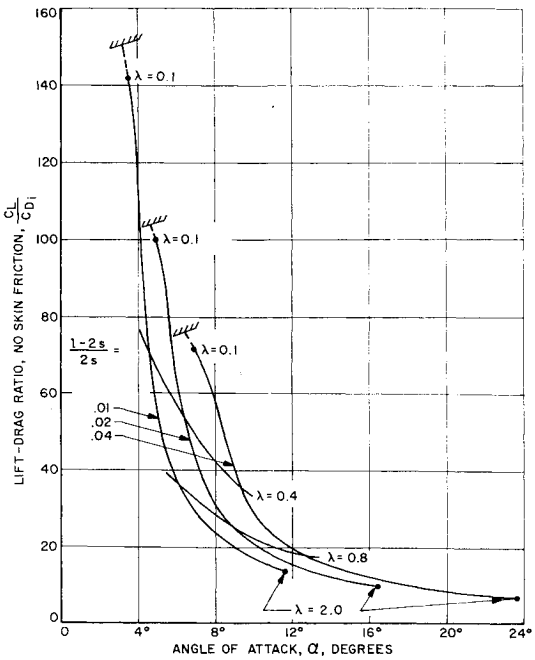

Fig. 8 Induced-drag characteristics of one-lobed parawing with 20° semiapex angle.

Table 5 Nondimensional characteristics of slender one-lobed delta parawings: span loading distributions, $cc_l/(cc_l)_{y=0}$

	y/s							
λ	0	0.2	0.4	0.6	0.8	0.9	0.95	1.0
0.1	1.000	0.902	0.613	0.186	−0.162	−0.176	−0.125	0
0.2	1.000	0.941	0.768	0.494	0.181	0.0542	0.0124	0
1.0	1.000	0.972	0.888	0.742	0.516	0.355	0.245	0
2	1.000	0.976	0.902	0.771	0.559	0.395	0.278	0
10	1.000	0.979	0.914	0.794	0.592	0.428	0.305	0
100	1.000	0.980	0.916	0.799	0.599	0.435	0.312	0
Elliptical loading	1.000	0.980	0.916	0.800	0.600	0.436	0.312	0

the root chord. Table 6 illustrates this tendency. The limiting shape of the parawing at $\lambda = 0$ is

$$\frac{\eta}{s} = \frac{\sin\alpha}{\tan\epsilon}\left(1 - \frac{y}{s}\right) \qquad 0 \leq \frac{y}{s} \leq 1$$

$$\frac{\eta}{s} = \frac{\sin\alpha}{\tan\epsilon}\left(1 + \frac{y}{s}\right) \qquad -1 \leq \frac{y}{s} \leq 0$$

At $y/s = 0$ there is thus a sudden discontinuity in the derivative $\partial\eta/\partial y$ from positive to negative. Since the loading is given by the equation

$$\Delta p = -T(\partial^2\eta/\partial y^2)$$

the loading is zero everywhere except at the root chord, where a delta function in the loading exists. It is easy to evaluate the lift caused by such a loading assuming flat surfaces and small tensions. We thus find

$$\frac{C_L}{\tan\epsilon \sin\alpha} = 8\lambda \qquad \lambda \text{ very small}$$

This result is also found by evaluating the lift from the tension and the shapes of the wing at $y/s = \pm 1$.

3.3 Specific Results for 20° Semiapex Angle

Although the behavior of one-lobed parawings as a class have some interesting properties, it is of further interest to look at the aerodynamic characteristics of a specific wing of the class. These characteristics are obtained by assuming a semiapex angle ϵ and then computing all other quantities for fixed values of slack as a function of λ.

Consider the lift characteristics shown in Fig. 7. Lines of constant tension λ and of constant slack $[(l - 2s)/(2s)]$ are shown in the figure. For no slack and infinite tension we have a flat slender delta wing with lift-curve slope $(\pi/2)AR$. For all fixed values of the slack, the lift-curve slope is not greatly different from $(\pi/2)AR$, although some nonlinearity in lift curve is seen.

The ratio of lift to induced drag has been calculated and is shown in Fig. 8 for several values of the slack. The lift-drag ratio is greatest for small angles of attack and small tensions. Its value is limited, however, by the positive angles of zero lift, at which the curves in the figure are terminated. At a fixed angle of attack, the lift-drag ratio increases as the slack increases. Unlike a flat plate, the parawing does not approach an infinite value of C_L/C_{D_i} as α approaches α_0, because the span loading does not remain elliptical but tends to be concentrated at the root chord.

Table 6 Nondimensional characteristics of slender one-lobed delta parawings: shapes for small λ, $(\eta/s)(\tan\epsilon/\sin\alpha)$

y/s	$\lambda = 10^{-1}$, $n = 20$	$\lambda = 10^{-2}$, $n = 45$	$\lambda = 10^{-3}$, $n = 45$	$\lambda = 0$, $n = 45$	$1 - y/s$
0	0.7400	0.8791	0.9443	0.9826	1.0000
0.1	0.7335	0.8649	0.9116	0.9006	0.9000
0.2	0.7137	0.8192	0.8016	0.8041	0.8000
0.3	0.6796	0.7346	0.6998	0.7069	0.7000
0.4	0.6297	0.6130	0.5993	0.6090	0.6000
0.5	0.5621	0.4966	0.4986	0.5106	0.5000
0.6	0.4752	0.4053	0.3983	0.4122	0.4000
0.7	0.3689	0.3005	0.2981	0.3133	0.3000
0.8	0.2467	0.1995	0.1978	0.2140	0.2000
0.9	0.1183	0.1000	0.0978	0.1141	0.1000
1.0	0	0	0	0	0

References

[1] Thwaites, B., "The aerodynamic theory of sails. I. Two-dimensional sails," Proc. Roy. Soc. **261**, 402–422 (1961).

[2] Nielsen, J. N., "Theory of flexible aerodynamic surfaces," J. Appl. Mech. **30**, 435–442 (1963).

[3] Nielsen, J. N., Kriebel, A. R., and Goodwin, F. K., "Theoretical aerodynamics of flexible wings at low speeds. I—One-lobed parawings," Vidya Rept. 84 (1962), Armed Services Technical Information Agency Rept. (AD 422 736).

[4] Nielsen, J. N., *Missile Aerodynamics* (McGraw-Hill Book Co., Inc., 1960), p. 48.

[5] Glauert, H., *Aerofoil and Airscrew Theory* (The MacMillan Co., New York, 1943), pp. 138–160.

[6] Jones, R. T. and Cohen, D., *High Speed Wing Theory* (Princeton University Press, Princeton, N. J., 1960); also Princeton Aeronautical Paperbacks 6, pp. 23–24.

[7] Timoshenko, S. and Woinowsky-Krieger, S., *Theory of Plates and Shells* (McGraw-Hill Book Co., Inc., New York, 1959), p. 461.